8. Ueta, M. *et al.* in *Excitonic Processes in Solids* Ch. 3 (Springer, Berlin, 1986).
9. Itoh, T. & Suzuki, T. Excitonic polariton-polariton resonance scattering via excitonic molecules in CuCl. *J. Phys. Soc. Jpn* **45,** 1939–1948 (1978).
10. Hönerlage, B. *et al.* The dispersion of excitons, polaritons and biexcitons in direct-gap semiconductors. *Phys. Rep.* **124,** 161–253 (1985).
11. Kuwata, M., Mita, T. & Nagasawa, N. Polarization rotation effects associated with the two-photon transition of Γ_1 excitonic molecules in CuCl. *Opt. Commun.* **40,** 208–211 (1982).
12. Savasta, S., Martino, G. & Girlanda, R. Entangled photon pairs from the optical decay of biexcitons. *Solid State Commun.* **111,** 495–500 (1999).
13. Shimano, R., Svirko, Y. P., Mysyrowicz, A. & Kuwata-Gonokami, M. Efficient two-photon light amplification by a coherent biexciton wave. *Phys. Rev. Lett.* **89,** 233601 (2002).
14. Saba, M. *et al.* High-temperature ultrafast polariton parametric amplification in semiconductor microcavities. *Nature* **414,** 731–735 (2001).
15. James, D. F. V., Kwiat, P. G., Munro, W. J. & White, A. G. Measurement of qubits. *Phys. Rev. A* **64,** 052312 (2001).
16. White, A. G., James, D. F. V., Munro, W. J. & Kwiat, P. G. Exploring Hilbert space: Accurate characterization of quantum information. *Phys. Rev. A* **65,** 01230 (2001).
17. Munro, W. J., Nemoto, K. & White, A. G. The Bell inequality: a measure of entanglement? *J. Mod. Opt.* **48,** 1239–1246 (2001).
18. Boto, A. N. *et al.* Quantum interferometric optical lithography: exploiting entanglement to beat the diffraction limit. *Phys. Rev. Lett.* **85,** 2733–2736 (2000).
19. Walter, P. *et al.* De Broglie wavelength of a non-local four-photon state. *Nature* **429,** 158–161 (2004).
20. Mitchell, M. W., Lundeen, J. S. & Steinberg, A. M. Super-resolving phase measurements with a multiphoton entangled state. *Nature* **429,** 161–164 (2004).

Acknowledgements We thank M. Hasegawa for his help in preparing samples. K.E. is grateful to P. G. Kwiat, M. Kuwata-Gonokami and H. Ishihara for discussions. This work was supported in part by the programme "Strategic Information and Communications R & D Promotion Scheme" of the Ministry of Public Management, Home Affairs, Posts and Telecommunications of Japan.

Competing interests statement The authors declare that they have no competing financial interests.

Correspondence and requests for materials should be addressed to K.E. (eda@riec.tohoku.ac.jp).

A high-performance cathode for the next generation of solid-oxide fuel cells

Zongping Shao & Sossina M. Haile

Materials Science, California Institute of Technology, Pasadena, California 91125, USA

Fuel cells directly and efficiently convert chemical energy to electrical energy[1]. Of the various fuel cell types, solid-oxide fuel cells (SOFCs) combine the benefits of environmentally benign power generation with fuel flexibility. However, the necessity for high operating temperatures (800–1,000 °C) has resulted in high costs and materials compatibility challenges[2]. As a consequence, significant effort has been devoted to the development of intermediate-temperature (500–700 °C) SOFCs. A key obstacle to reduced-temperature operation of SOFCs is the poor activity of traditional cathode materials for electrochemical reduction of oxygen in this temperature regime[2]. Here we present $Ba_{0.5}Sr_{0.5}Co_{0.8}Fe_{0.2}O_{3-\delta}$ (BSCF) as a new cathode material for reduced-temperature SOFC operation. BSCF, incorporated into a thin-film doped ceria fuel cell, exhibits high power densities (1,010 mW cm^{-2} and 402 mW cm^{-2} at 600 °C and 500 °C, respectively) when operated with humidified hydrogen as the fuel and air as the cathode gas. We further demonstrate that BSCF is ideally suited to 'single-chamber' fuel-cell operation, where anode and cathode reactions take place within the same physical chamber[3]. The high power output of BSCF cathodes results from the high rate of oxygen diffusion through the material. By enabling operation at reduced temperatures, BSCF cathodes may result in widespread practical implementation of SOFCs.

The primary function of the cathode in a fuel cell based on an oxygen-conducting electrolyte is to facilitate the multistep electrochemical reduction of oxygen[4]:

$$1/2\ O_2\ (\text{gas}) + 2e^-\ (\text{cathode}) \rightarrow O^{2-}\ (\text{electrolyte}) \qquad (1)$$

In a single-chamber fuel cell, the cathode must furthermore be inactive towards oxidation of fuel, and operation at reduced temperatures is essential to minimize undesirable gas-phase reactions[2] (Supplementary Fig. 1). In the present work, we use BSCF as a new cathode material and demonstrate excellent performance in both dual-chamber and single-chamber configurations at temperatures lower than 600 °C. This material, a cubic perovskite (Supplementary Fig. 2) in the $BaCoO_{3-\delta}$–$SrCoO_{3-\delta}$ system, was first developed as a high-temperature (>800 °C) oxygen permeation membrane material[5,6]. Unlike typical cathodes, the A-site cation of BSCF perovskite is an alkaline-earth species rather than a rare-earth element.

We first measured the polarization resistance of BSCF by two-electrode impedance methods using symmetric BSCF|electrolyte|BSCF cells, where the electrolyte was ~1-mm-thick 15 mol% samaria-doped ceria (SDC). As is standard in this field, we use the term area specific resistance (ASR) to describe all resistance terms associated with the electrode, whether they occur at the gas–cathode interface, within the bulk of the cathode, or at the cathode–electrolyte interface. Data were collected under a uniform air atmosphere, both with (three-electrode) and without (two-electrode) a reference electrode; the three-electrode configuration allowed direct measurement of the half-cell voltage with and without an applied direct current. The cathode ASR (Fig. 1a) was determined from raw impedance plots as indicated in Fig. 1b, where the high-frequency offset is due primarily to the electrolyte resistance and the radius of the complete arc to the cathode resistance. The ASR, as determined by both techniques, was remarkably low: 0.055–0.071 Ω cm^2 at 600 °C, and 0.51–0.60 Ω cm^2 at 500 °C. Furthermore, the measured value dropped from ~0.60 Ω cm^2 to ~0.27 Ω cm^2 at 500 °C under an applied current of 0.14 A cm^{-2}. Cells fabricated using silver alone as the cathode showed ASR values ~1,000 times larger (Supplementary Fig. 3), demonstrating that silver paste, used to attach silver mesh leads, served only as a current collector. The ASR of the BSCF cathode reported here is substantially lower than that of other single-phase perovskite cathodes measured under similar conditions, and comparable to that of the best composite systems[7–10].

The performance of the BSCF cathode in a conventional, dual-chamber fuel cell was then investigated, again using SDC as the electrolyte. A thin (20 μm) electrolyte layer was supported on a 700-μm-thick Ni + SDC anode, with a 10–20-μm-thick BSCF cathode layer deposited on the opposing side, after first depositing an additional porous interlayer of SDC (<5 μm in thickness). Air was supplied to the cathode chamber and humidified H_2 (3% H_2O) to the anode chamber. Peak power densities of ~1,010 mW cm^{-2} and 402 mW cm^{-2} were obtained at respectively 600 °C and 500 °C (Fig. 2a). These values are more than twice those measured in our laboratory for a similar cell but with SSC + SDC as cathode (Supplementary Fig. 4). In addition to the polarization curves, the cell resistances under open-circuit conditions were measured at various temperatures by impedance spectroscopy. The electrode polarization resistance (the sum of anode and cathode ASRs) is only about 0.021 Ω cm^2 at 600 °C, and 0.135 Ω cm^2 at 500 °C (Fig. 2), amounting to just 14% and 26% of the resistance of electrolyte at these respective temperatures (Supplementary Fig. 5). It is noteworthy that composite SDC + BSCF cathodes, although still very active for oxygen electroreduction, yielded lower power densities than simple BSCF cathodes.

The trilayer fuel cell was further operated in a single-chamber configuration with a propane + O_2 + He mixture in a 4:9:36 volumetric ratio as the feed gas, and a total flow rate of

490 ml min^{-1}. A peak power density of ~391 mW cm^{-2} was observed at a furnace set temperature of 575 °C, with a current density at short circuit of ~1.9 A cm^{-2}. At 525 °C the respective values were ~ 358 mW cm^{-2} and ~1.7 A cm^{-2}. Upon modifying the BSCF cathode to incorporate 30 wt% SDC, significant improvements in power density were observed in single-chamber mode over simple BSCF. At a furnace set temperature of 500 °C, a peak power density of ~440 mW cm^{-2} was achieved (Fig. 3). Hibino *et al.*[3] reported a comparably high peak power density of 403 mW cm^{-2} at 500 °C for an electrolyte-supported fuel cell using SSC + SDC as the cathode and ethane as the fuel. However, this cathode was incompatible with propane at temperatures higher than 450 °C (ref. 3). It should be noted that, because of the heat release during partial oxidation at that anode, the real temperature of the single-chamber fuel cell is about 150–245 °C higher than the furnace temperature, depending on the operation conditions (Supplementary Fig. 6). This self-heating in SCFC mode explains the higher power densities obtained from single-chamber than from dual-chamber fuel cells at nominally low temperatures (compare Figs 2a and 3).

The mechanisms responsible for the excellent performance of BSCF as a fuel-cell cathode were identified by oxygen permeability measurements (Supplementary Figs 7–9) and extensive impedance spectroscopy studies of symmetric cells (Supplementary Figs 10, 11). The oxygen permeation measurements, combined with thermal gravimetric analysis to determine the oxygen vacancy concentration as a function of oxygen partial pressure, revealed that the oxygen vacancy diffusion rate is 7.3×10^{-5} cm^2 s^{-1} at 775 °C and 1.3×10^{-4} cm^2 s^{-1} at 900 °C (temperatures at which such measurements could be accurately performed), from 2 to 200 times greater than that of comparable cathode perovskites[11,12]. In addition, the activation energy for oxygen diffusion in BSCF was found to be less than half that for oxygen surface exchange, 46 ± 2 kJ mol^{-1} versus 113 ± 11 kJ mol^{-1}, suggesting that oxygen surface exchange is the rate-limiting step at low temperatures and that the exceptionally high oxygen diffusivity through BSCF gives it its overall high rate of oxygen electro-oxidation. The oxygen ion conductivity is, in fact, higher than that of SDC. It is for this reason that introduction of a small amount of the electrolyte material decreases cathode performance in dual-chamber configuration, rather than increasing it, as is otherwise observed (for example, in composite LSM + YSZ cathodes[13]).

Impedance spectroscopy of the symmetric cells strongly supported the conclusions of the permeability measurements: specifically, that oxygen diffusion is rapid and surface exchange kinetics are

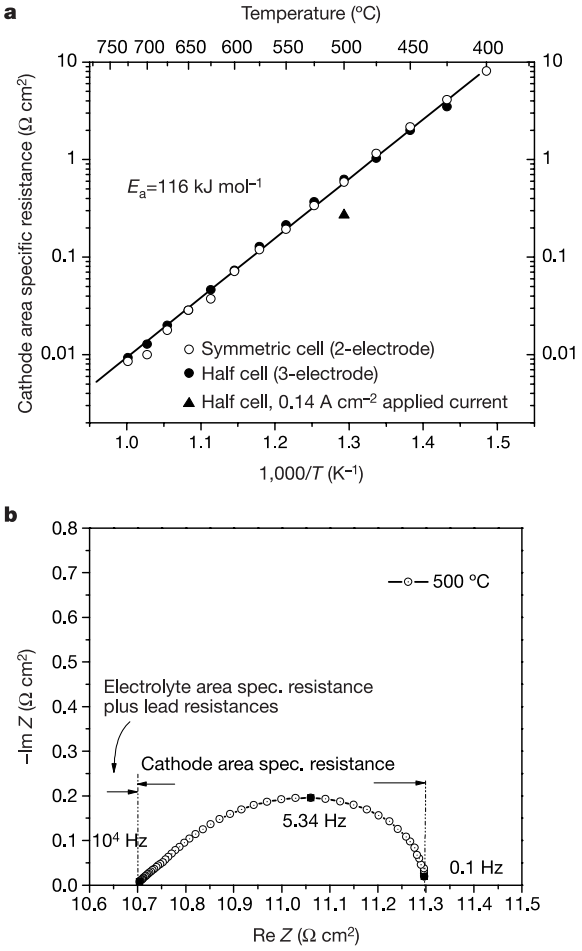

Figure 1 The area specific resistance (ASR) of the cathode material BSCF under air, measured both with (three-electrode, half cell) and without (two-electrode, symmetric cell) a reference electrode. **a**, ASR as a function of temperature, and **b**, a typical impedance spectrum, as obtained from the two-electrode, symmetric cell at 500 °C (raw impedance data have been multiplied by the fuel-cell active area, 0.71 cm^2, so that the cathode ASR corresponds directly to the diameter of the arc associated with the cathode response). The electrolyte, 15 mol% samaria-doped ceria (SDC), is about 1 mm thick, and each electrode about 20 μm thick. The activation energy for the overall cathode resistance is 116 kJ mol^{-1}, comparable to that determined for the surface exchange process, indicating that surface exchange at the cathode–air interface is the rate-limiting step.

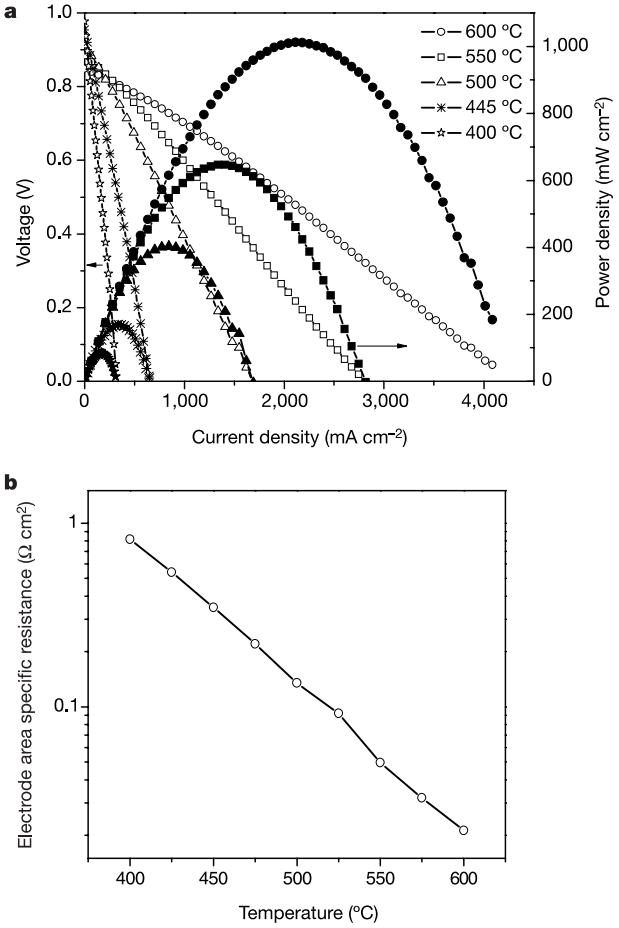

Figure 2 Performance obtained from a $Ba_{0.5}Sr_{0.5}Co_{0.8}Fe_{0.2}O_{3-\delta}$ (~20 μm)|$Sm_{0.15}Ce_{0.85}O_{2-\delta}$ (~20 μm)|Ni + $Sm_{0.15}Ce_{0.85}O_{2-\delta}$ (~700 μm) fuel cell. Air was supplied to the cathode (400 ml min^{-1} at STP) and 3% H_2O-humidified H_2 was supplied to the anode (80 ml min^{-1} at STP). **a**, Cell voltage and power density as functions of current density, and **b**, ASRs of the electrodes (sum of anode and cathode contributions) measured under open circuit conditions. The peak power density reaches 1 W cm^{-2} at 600 °C.

rate-limiting. In particular, (1) good linearity of the cathode ASR versus reciprocal temperature was observed over the temperature range investigated, 400–725 °C, and the derived activation energy, ~116 kJ mol^{-1}, was almost identical to that determined for the oxygen surface exchange step (113 ± 11 kJ mol^{-1}). (2) At low temperatures, the cathode ASR was sensitive to the presence of CO_2 and H_2O in the atmosphere, gases which could only affect surface and not bulk properties. Carbon dioxide increased the interfacial resistance whereas steam decreased it (Supplementary Fig. 10). (3) An increase in the cathode thickness decreased the ASR (without changing the activation energy) (Supplementary Fig. 11), presumably as a result of increasing the area over which surface exchange could occur. (4) The possibility that interfacial charge transfer could be the rate-limiting step is eliminated by the fact that no arc that could be associated with this step appeared in the impedance data.

The observation that the apparent cathode ASR drops under applied current (without detectable changes in structure as determined by *ex situ* X-ray diffraction), Fig. 1a, is additionally consistent with a picture in which the surface exchange step is rate-limiting. Specifically, it is known that oxygen adsorption and desorption rates can differ significantly, with desorption occurring much more slowly than adsorption[14]. In the absence of an applied current there is no net ion flux, and thus the adsorption and desorption processes contribute equally to the measured resistance. Under an applied current, however, net adsorption occurs at the electrode functioning as the cathode, and the measured rate is dominated by this faster process, resulting in the observed reduction in ASR. Such an effect could not occur for an overall process limited by bulk diffusion.

A key characteristic of a useful cathode for single-chamber fuel-cell applications is a low activity towards fuel oxidation under the oxidant + fuel environment. It is notable that, together with its high activity of oxygen electroreduction, BSCF exhibits the quality of low activity towards propane oxidation. Under stoichiometric conditions (O_2:C_3H_8 = 5:1 with 95 vol.% helium) and at 500 °C, the propane conversion rates over BSCF, LSCF and SSC are 5.3%, 35.5% and 16.1%, respectively (Fig. 4). The high activity of SSC towards propane oxidation is probably responsible for the relatively poor performance of this cathode[3]. Incorporation of electrolyte material into the BSCF cathode under the single-chamber fuel-cell configuration improves performance (unlike the dual-chamber results), and we speculate that the electrolyte is beneficial for limiting the detrimental influence of *in situ* generated CO_2 on the oxygen surface exchange kinetics of BSCF.

For practical applications, in addition to high power density, good fuel-cell stability is essential. Degradation can occur either by reduction/phase decomposition under low oxygen partial pressures or by phase segregation under an oxygen partial pressure gradient. Whereas phase segregation under a steep oxygen concentration gradient has been reported for BSCF[5,15], such conditions are unlikely to exist in the fuel-cell cathode because of rapid oxygen diffusion through BSCF. Furthermore, we found that reduction of BSCF occurs only at oxygen partial pressures of $<10^{-6}$–10^{-8} atm. These partial pressures are equivalent to cathode polarization drops of 0.20–0.23 V at 500–600 °C for a cell exposed to ambient air at the cathode. At lower temperatures, polarization losses increase, as does the tendency towards phase segregation, and thus stability at low temperatures provides a stringent measure of long-term viability. A preliminary examination of stability was carried out using a dual-chamber fuel cell with a BSCF-based cathode, operated at 390 °C under an air/3% humidified H_2 gradient. The cell showed essentially stable performance within the test period of 120 h (Supplementary Fig. 12). Under the fuel-rich, single-chamber conditions employed above, the thermodynamic oxygen partial pressure is as low as 10^{-28} atm at 500 °C, conditions that could well induce the reduction of BSCF. Because such reduction was not observed in our experiments, we conclude that the poor activity of BSCF for propane oxidation results in local oxygen partial pressures in the vicinity of the cathode which are high enough to prevent reduction of cobalt.

The present study demonstrates that very high power densities can be achieved at low temperatures in both dual-chamber and single-chamber fuel cells using $Ba_{0.5}Sr_{0.5}Co_{0.8}Fe_{0.2}O_{3-\delta}$ as a cathode. A significant fraction of the overall cell resistance even at 500 °C (~74%) in dual-chamber configuration is attributable to the 20-μm-thick electrolyte. The SDC used here has a measured conductivity of ~4.7×10^{-3} S cm^{-1} at 500 °C (Supplementary Fig. 5), which is lower than the best reported value for doped ceria, ~9.5×10^{-3} S cm^{-1} (ref. 16). Thus, a decrease in electrolyte resist-

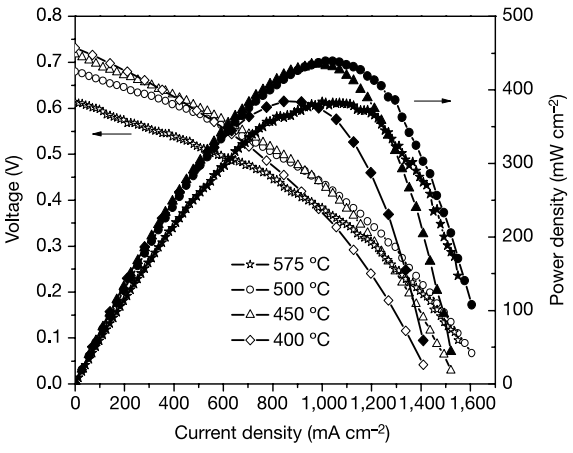

Figure 3 Cell voltage and power density as functions of current density obtained in single-chamber mode from a $Ba_{0.5}Sr_{0.5}Co_{0.8}Fe_{0.2}O_{3-\delta}$ + $Sm_{0.15}Ce_{0.85}O_{2-\delta}$ (~20 μm)|$Sm_{0.15}Ce_{0.85}O_{2-\delta}$ (~20 μm)|Ni + $Sm_{0.15}Ce_{0.85}O_{2-\delta}$ (~700 μm) fuel cell. The BSCF:SDC ratio in the cathode was 70:30 by weight. A mixture of propane, oxygen and helium, flowing (at STP) at 40 ml min^{-1}, 90 ml min^{-1} and 360 ml min^{-1}, respectively, was used as the feed gas. The temperature reported is that of the furnace; local heating due to partial oxidation at the anode can result in considerably higher temperatures ($\Delta T \approx$ 188–240 °C, Supplementary Fig. 6). The peak power density is relatively insensitive to furnace temperature, broadly peaking at 500 °C at a value of ~440 mW cm^{-2}.

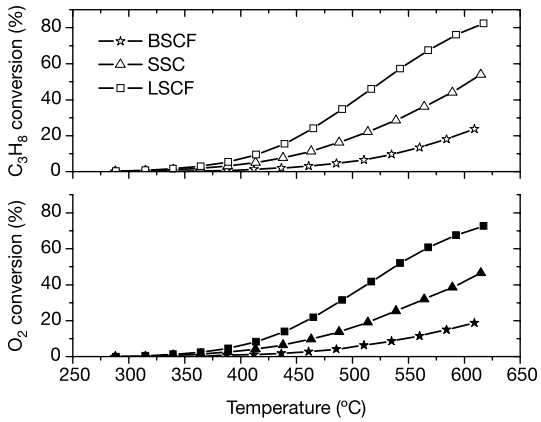

Figure 4 Comparison of the catalytic activities of BSCF ($Ba_{0.5}Sr_{0.5}Co_{0.8}Fe_{0.2}O_{3-\delta}$), SSC ($Sm_{0.5}Sr_{0.5}CoO_{3-\delta}$), and LSCF ($La_{0.6}Sr_{0.4}Co_{0.2}Fe_{0.8}O_{3-\delta}$) oxides towards propane oxidation under stoichiometric conditions. Test samples were exposed to a mixture of propane, oxygen and helium flowing (at STP) at 40 ml min^{-1}, 90 ml min^{-1} and 360 ml min^{-1}, respectively. Powders were calcined for 5 h at appropriate temperatures so as to yield comparable specific surface areas: BSCF at 900 °C (0.62 m^2 g^{-1}), SSC at 1,050 °C (0.66 m^2 g^{-1}) and LSCF at 1,100 °C (0.65 m^2 g^{-1}). Low catalytic activity of BSCF is advantageous for single-chamber fuel-cell operation.

ance by a factor of two could realistically be achieved by optimization of its synthesis and composition, or by reduction of its thickness to ~10 μm (as has already been achieved in the literature[17]), and can be anticipated to result in a peak power density of >600 mW cm^{-2} at 500 °C. Additional increases in power density may be achieved through precise control of the cathode architecture using advanced preparation methods to maximize the surface area over which the oxygen exchange reaction can occur. These steps would probably also yield benefits for operation under single-chamber fuel-cell mode. In addition, a detailed study of possible degradation due to phase segregation induced by the oxygen flux through the cathode, particularly at high current densities, may be necessary for evaluating the long-term viability of BSCF cathodes.□

Methods

Cathode powder preparation

Phase-pure $Ba_{0.5}Sr_{0.5}Co_{0.8}Fe_{0.2}O_{3-\delta}$, $Sm_{0.5}Sr_{0.5}CoO_{3-\delta}$ and $La_{0.6}Sr_{0.4}Co_{0.2}Fe_{0.8}O_{3-\delta}$ powders were synthesized by a sol–gel method in which the appropriate metal nitrates were dissolved in water, and a combination of EDTA and citric acid served as complexing agents. Mild heating induced gelation of the solution, and the resulting gel was held at 250 °C for 12 h to remove organics, and then calcined for 5 h under stagnant air at 900–1,050 °C.

Fuel-cell fabrication

Electrolyte-supported symmetric cells for impedance studies were prepared by nitrogen-borne spray deposition of BSCF powder suspended in isopropyl alcohol onto both sides of an SDC electrolyte disk (~1 mm), followed by calcination at 1,000 °C for 5 h under stagnant air. Silver mesh was attached to the electrode surfaces using silver paste as the current collector. Anode-supported thin-film electrolyte fuel cells (trilayer cells) were fabricated using a dual dry-pressing method. The anode, formed from a 60:40 wt% mixture of NiO and SDC powders was dry-pressed into a pellet, and then an electrolyte powder was distributed on the anode surface and co-pressed with the anode. The resultant bilayer was calcined at 1,350 °C for 5 h in air, and then reduced at 600 °C under flowing hydrogen for 5 h. Either simple BSCF or a 70:30 (by weight) BSCF + SDC powder mixture dispersed in isopropyl alcohol was sprayed on the electrolyte surface. The cell was calcined at 1,000 °C for 5 h under flowing nitrogen. The final fuel cells had the following properties: diameter of 1.33 cm, anode thickness of 0.7 mm, anode porosity of ~46%, electrolyte thickness of ~20 μm, cathode thickness of 10–20 μm, and cathode porosity of ~30%.

Fuel-cell electrochemical characterization

Both symmetric cells and complete trilayer fuel cells were placed in an in-house constructed measurement station, and polarization curves collected using a Keithley 2420 source meter based on the four-probe configuration. In the case of dual-chamber measurements, the trilayer cell was sealed to a quartz tube using silver paste, the cathode side was open to air, and the anode side was exposed to 3% H_2O-humidified H_2 at a flow rate of 80 ml min^{-1} at STP. For the single-chamber fuel-cell test, the whole cell was place in a quartz tube reactor with an inner diameter of 15 mm. Digital mass flow controllers (Aera FC-D980C) were used to introduce propane, oxygen and helium gases to the reactor at various flow rates.

Electrochemical impedance test

The ASR of BSCF cathode was measured in the two-electrode symmetric cell configuration under air. Impedance measurements were performed using a Solartron 1260A frequency analyser under open circuit conditions from 10 mHz to 10^5 Hz. The three-electrode half-cell test was conducted by fixing an additional silver electrode to the middle edge of the SDC as a reference electrode, and then measuring the impedance between the working and reference electrodes measured under both open circuit conditions and current polarization conditions using a combined Solartron 1260A frequency response analyser and a PAR EG&G 273A potentiostat/galvanostat. The impedance of the single cell was also measured under asymmetric atmospheres under open circuit conditions.

Catalytic activity

The catalytic activity of BSCF and other cathode materials towards propane oxidation was tested in a flow-through quartz reactor with a 6 mm inner diameter, containing a fixed bed of 0.3 g catalyst mixed with 1.5 g of silica granules. A gas mixture of He + C_3H_8 + O_2 was passed through the reactor, which was heated to various temperatures using an electrical furnace. The effluent gas was analysed using an in-line Varian CP-4900 Micro GC.

Received 25 February; accepted 25 June 2004; doi:10.1038/nature02863.

1. Steel, B. C. H. & Heinzel, A. Materials for fuel-cell technologies. *Nature* **414,** 345–352 (2001).
2. Brandon, N. P., Skinner, S. & Steele, B. C. H. Recent advances in materials for fuel cells. *Annu. Rev. Mater. Res.* **33,** 183–213 (2003).
3. Hibino, T. *et al.* A low-operating-temperature solid oxide fuel cell in hydrocarbon-air mixtures. *Science* **288,** 2031–2033 (2000).
4. Fleig, J. Solid oxide fuel cell cathodes: Polarization mechanisms and modeling of the electrochemical performance. *Annu. Rev. Mater. Res.* **33,** 361–382 (2003).
5. Shao, Z. P. *et al.* Investigation of the permeation behavior and stability of a $Ba_{0.5}Sr_{0.5}Co_{0.8}Fe_{0.2}O_{3-\delta}$ oxygen membrane. *J. Membr. Sci.* **172,** 177–188 (2000).
6. Shao, Z. P., Dong, H., Xiong, G. X., Cong, Y. & Yang, W. S. Performance of a mixed-conducting ceramic membrane reactor with high oxygen permeability for methane conversion. *J. Membr. Sci.* **183,** 181–192 (2001).
7. Huang, K., Wan, J. & Goodenough, J. B. Increasing power density of LSGM-based solid oxide fuel cells using new anode materials. *J. Electrochem. Soc.* **148,** A788–A794 (2001).
8. Ishihara, T., Fukui, S., Nishiguchi, H. & Takita, Y. La-doped $BaCoO_3$ as a cathode for intermediate temperature solid oxide fuel cells using a $LaGaO_3$ based electrolyte. *J. Electrochem. Soc.* **149,** A823–A828 (2002).
9. Ralph, J. M., Rossignol, C. & Kumar, R. Cathode materials for reduced-temperature SOFCs. *J. Electrochem. Soc.* **150,** A1518–A1522 (2003).
10. Xia, C. R. & Liu, M. L. Novel cathodes for low-temperature solid oxide fuel cells. *Adv. Mater.* **14,** 521–523 (2002).
11. Kim, S., Yang, Y. L., Jacobson, A. J. & Abeles, B. Diffusion and surface exchange coefficients in mixed ionic and electronic conducting oxides from the pressure dependence of oxygen permeation. *Solid State Ionics* **106,** 189–195 (1998).
12. Xu, S. J. & Thomson, W. J. Oxygen permeation rates through ion-conducting perovskite membranes. *Chem. Eng. Sci* **54,** 3839–3850 (1999).
13. Tsai, T. & Barnett, S. A. Effect of LSM-YSZ cathode on thin-electrolyte solid oxide fuel cell performance. *Solid State Ionics* **93,** 207–217 (1997).
14. Fukunaga, H., Koyama, M., Takahashi, N., Wen, C. & Yamada, K. Reaction model of dense $Sm_{0.5}Sr_{0.5}CoO_3$ as SOFC cathode. *Solid State Ionics* **132,** 279–285 (2000).
15. van Veen, A. C., Rebeilleau, M., Farrusseng, D. & Mirodatos, C. Studies on the performance stability of mixed conducting BSCFO membranes in medium temperature oxygen permeation. *Chem. Commun.*, 32–33 (2003).
16. Steele, B. C. H. Appraisal of $Ce_{1-y}Gd_yO_{2-y/2}$ electrolytes for IT-SOFC operation at 500 °C. *Solid State Ionics* **129,** 95–110 (2000).
17. Xia, C. R. & Liu, M. L. A simple and cost-effective approach to fabrication of dense ceramic membranes on porous substrates. *J. Am. Ceram. Soc.* **84,** 1903–1905 (2001).

Supplementary Information accompanies the paper on **www.nature.com/nature**.

Acknowledgements This work was funded by the Defense Advanced Research Projects Agency, Microsystems Technology Office. Additional support was provided by the National Science Foundation through the Caltech Center for the Science and Engineering of Materials. Selected oxygen permeability measurements were carried out in the Laboratory of Reaction Engineering and Energy, Institute of Research on Catalysis, CNRS, France, during the visit of Z.P.S. there, hosted by C. Mirodatos.

Competing interests statement The authors declare that they have no competing financial interests.

Correspondence and requests for materials should be addressed to S.M.H. (smhaile@caltech.edu).

The transition to a sulphidic ocean ~1.84 billion years ago

Simon W. Poulton[1], Philip W. Fralick[2] & Donald E. Canfield[1]

[1]*Danish Center for Earth System Science, Institute of Biology, University of Southern Denmark, Campusvej 55, 5230 Odense M, Denmark*
[2]*Department of Geology, Lakehead University, Thunder Bay, Ontario P7B 5E1, Canada*

The Proterozoic aeon (2.5 to 0.54 billion years (Gyr) ago) marks the time between the largely anoxic world of the Archean (>2.5 Gyr ago)[1] and the dominantly oxic world of the Phanerozoic (<0.54 Gyr ago). The course of ocean chemistry through the Proterozoic has traditionally been explained by progressive oxygenation of the deep ocean in response to an increase in atmospheric oxygen around 2.3 Gyr ago. This postulated rise in the oxygen content of the ocean is in turn thought to have led to the oxidation of dissolved iron, Fe(II), thus ending the deposition of banded iron formations (BIF) around 1.8 Gyr ago[1,2]. An alternative interpretation suggests that the increasing atmospheric oxygen levels enhanced sulphide weathering on land and the flux of sulphate to the oceans. This increased rates of sulphate reduction, resulting in Fe(II) removal in the form of pyrite as the oceans became sulphidic[3]. Here we investigate sediments from the ~1.8-Gyr-old Animikie group, Canada, which were deposited during the final stages of the main global period of BIF